Theoretical analysis of the dimensionality of ultrasonic attenuation in polycrystalline materials with elongated grains

Juan Camilo Victoria Giraldo, Bing Tie, Jérôme Laurent, Alain Lhémery, Denis Solas

Theoretical analysis of the dimensionality of ultrasonic attenuation in polycrystalline materials with elongated grains

Juan Camilo Victoria Giraldo[1], Bing Tie[1], Jérôme Laurent[2], Alain Lhémery[2] and Denis Solas[3]

[1] Université Paris-Saclay, CentraleSupélec, ENS Paris-Saclay, CNRS, LMPS, Gif-Sur-Yvette, 91190, France
[2] Université Paris-Saclay, CEA List, Palaiseau, 91120, France
[3] Université Paris-Saclay, CNRS, ICMMO, Orsay, 91400, France

E-mail: juan-camilo.victoria-giraldo@centralesupelec.fr, bing-tie@centralesupelec.fr

Abstract. In the present work, the grain scattering-induced attenuation coefficient is obtained for longitudinal bulk waves in untextured cubic polycrystalline materials with elongated grains using proposed 2D and 3D theoretical models. These models are obtained based on previously developed 2D and 3D models for equiaxed grains. Comparison of the 2D and 3D models allows an analysis of the dimensionality of grain scattering-induced attenuation, which involves more complex mechanisms with elongated grains. In the higher stochastic scattering regime, both 3D and 2D longitudinal attenuations are found to be dependent on the grain size parallel to the wave propagation. In the Rayleigh scattering regime the 3D attenuation is volume dependent and in contrast, the 2D longitudinal attenuation is found to be cross-section dependent and is therefore helpful for identifying the 3D grain shape/rotation.

1. Introduction

Ultrasonic wave scattering is an interesting phenomenon in which the wave propagation is locally disturbed by heterogeneities. Indeed, in polycrystalline materials, the inhomogeneities can be summarized in the relative crystallographic misorientation from grain to grain and the possible presence of multiple phases. In particular, knowledge about the influence of these inhomogeneities (grain size and shape, degree of anisotropy, etc.) on ultrasonic attenuation and the correlation between them is essential, as microstructural information can be used to characterize material properties of importance to design non-destructive testing methods [1, 2].

Although ultrasonic attenuation has already been studied mainly in 3D and is known as a dimension-dependent physical phenomenon, it is still interesting to investigate the attenuation in the 2D dimension since it helps to understand better the particularities of 3D behavior. Until now, several 3D theoretical models have been developed, with earlier models devoting attention to the case of randomly oriented, cubic crystals and equiaxed grains with the introduction of a two-point correlation (TPC) spatial isotropic function. Stanke and Kino [3] introduced a unified theory that accounts for an order of multiple scattering, based on Karal and Keller's [4] approximation. Weaver [5], on the contrary, based his work on Dyson's equation which accounts for multiple

scattering by the First-Order-Smoothing Approximation of the "self-energy" operator. These two models also have led to extensions considering more general grain shapes. For instance, Ahmed *et al* [6] followed the work of Stanke and Kino [3] by introducing a transverse isotropic TPC function and obtaining results by numerical integration for cubic randomly oriented crystals. Yang *et al* [7], implemented a general anisotropic function in Weaver's [5] equations and obtained a closed-form expression. Also, Calvet and Margerin [8] proposed a spectral approach based on the work of Weaver [5] and Yang *et al* [7], obtaining results up to the geometric frequency regime. Amplitude attenuation estimated from numerical simulations has been also carried out. In the 3D dimension Huang *et al* [9] focused on the case of microstructures with equiaxed grains and elongated grains [10]. Van Pamel *et al* [11] also carried out numerical simulations in microstructures with equiaxed grains, they did a comparison between 1D, 2D and 3D ultrasonic scattering and were able to find the power law dependency k^{D+1} in the Rayleigh scattering regime and k^2 in the stochastic regime.

Few works have dealt with 2D ultrasonic scattering, which remains an interesting problem insofar as it makes it possible to compare 2D and 3D models, to analyze the dimensionality of grain scattering phenomena, and to better understand their underlying mechanisms. In this work, Bai and Tie's model [12, 13] for bulk waves is recalled and then extended to the general case of elongated grains of ellipsoidal shape for the 2D and 3D cases. Our theoretical model is used to study the ultrasonic attenuation in 2D with an approach to better understand and give insights on the usefulness and possibility of inversely estimating the grain's shape/rotation.

2. General theoretical ultrasonic attenuation framework

2.1. Bulk waves ultrasonic attenuation considering elongated grains

This work follows the theoretical studies according to the unified theory of Stanke and Kino [3]. The objective here is to recall the equations used as a framework and to extend the model of Bai and Tie [12, 13] to the case of elongated grains.

Considering an ensemble of possible inhomogeneous media made of the same single polycrystalline material and occupying $\Omega \subset \mathbf{R}^{dim}, dim = 2, 3$. The polycrystalline material is defined by a position-dependent elastic tensor $\boldsymbol{C}(\boldsymbol{x})$ and a constant density ρ. The elastodynamic wave equation is known to be:

$$\boldsymbol{L}\left(\boldsymbol{u}(\boldsymbol{x},\omega)\right) = \rho\omega^2\boldsymbol{u}(\boldsymbol{x},\omega) + \nabla_x\left(\boldsymbol{C}(\boldsymbol{x}) : \boldsymbol{\varepsilon}(\boldsymbol{u}(\boldsymbol{x},\omega))\right) = \boldsymbol{0}. \tag{1}$$

We can then search for the solution by decomposing the wave equation operator into an operator defined in a homogeneous reference medium and an operator defined in a heterogeneous perturbation medium, defined as the deviation of the original heterogeneous medium from the reference medium $\delta\boldsymbol{C}(\boldsymbol{x}) = \boldsymbol{C}(\boldsymbol{x}) - \boldsymbol{C}^0$. The elastic tensor $\boldsymbol{C}^0$ is an equivalent homogeneous tensor chosen as the Voigt average [4], so $\langle\delta\boldsymbol{C}(\boldsymbol{x})\rangle = 0$. Furthermore, we consider the assumptions of a single-phase material and randomly oriented crystallographic axes, which means on average the medium $\boldsymbol{C}^0$ is isotropic. Also, assuming that the elastic tensor varies independently from grain to grain, the following simplification for the elastic autocorrelation function can be made $\langle\delta\boldsymbol{C}(\boldsymbol{x}) \otimes \delta\boldsymbol{C}(\boldsymbol{x'})\rangle = \langle\delta\boldsymbol{C}^g \otimes \delta\boldsymbol{C}^g\rangle W(\boldsymbol{r})$. Where $\delta\boldsymbol{C}^g$ is the elastic tensor variation which is constant in each grain. The average is considered to be the average overall crystallographic orientations, and the two-point correlation (TPC) spatial function $W(\boldsymbol{r})$ is the function responsible for the characteristic grain geometry description by estimating the probability of two random points $\boldsymbol{x}$ and $\boldsymbol{x'}$ are in the same grain, with $\boldsymbol{r} = \boldsymbol{x} - \boldsymbol{x'}$.

The idea is then to find the solution by assuming that the average propagating wave $\langle\boldsymbol{u}(\boldsymbol{x})\rangle$ has the form of a plane wave $\langle\boldsymbol{u}(\boldsymbol{x})\rangle = \boldsymbol{U}e^{ik\hat{\boldsymbol{k}}\cdot\boldsymbol{x}}$. With $\hat{\boldsymbol{k}}$ the unit wavevector and $\boldsymbol{U}$ the polarization vector. After considering the abovementioned simplifications in the second-order Karal and

Keller's approximation [4] we obtain a non-linear eigenvalue problem in the perturbed acoustic tensor $\boldsymbol{\Gamma}(k\hat{\boldsymbol{k}})$:

$$\boldsymbol{\Gamma}(k\hat{\boldsymbol{k}})\cdot\boldsymbol{U}=\rho\omega k^{-2}\boldsymbol{U}, \tag{2}$$

with:

$$\boldsymbol{\Gamma}(k\hat{\boldsymbol{k}})\cdot\boldsymbol{U}=\boldsymbol{\Gamma}^0(\hat{\boldsymbol{k}})\cdot\boldsymbol{U}+\delta\boldsymbol{\Gamma}(k\hat{\boldsymbol{k}})\cdot\boldsymbol{U}, \tag{3a}$$

$$\delta\boldsymbol{\Gamma}(k\hat{\boldsymbol{k}})\cdot\boldsymbol{U}=\Big(\Big(\langle\delta\boldsymbol{C}^g\otimes\delta\boldsymbol{C}^g\rangle:\boldsymbol{P}(k\hat{\boldsymbol{k}})\Big):(\hat{\boldsymbol{k}}\otimes_s\boldsymbol{U})\Big)\cdot\hat{\boldsymbol{k}}, \tag{3b}$$

$$\boldsymbol{\Gamma}^0(\hat{\boldsymbol{k}})\cdot\boldsymbol{U}=\Big(\boldsymbol{C}^0:(\hat{\boldsymbol{k}}\otimes_s\boldsymbol{U})\Big)\cdot\hat{\boldsymbol{k}}. \tag{3c}$$

One approach to solving the non-linear eigenvalue problem (2) for k is to assume that the propagating modes, in the case of weakly scattering media, can be assumed to be approximated by those pure modes of the reference homogeneous media $\boldsymbol{U}^0_\beta$ (i.e. $U^0_\beta||\hat{\boldsymbol{k}}$ for $\beta=L$, the case of a longitudinal mode or $U^0_\beta\perp\hat{\boldsymbol{k}}$ for $\beta=T$, the case of a transverse mode). Then, after applying the scalar product with $\boldsymbol{U}^0_\beta$ to both sides of (2), the following expression (4) for the propagation constant k_β can be obtained from the perturbed acoustic tensor:

$$k_\beta^2-k_{0\beta}^2=k_\beta^2\frac{\langle\delta C_{j^\beta jkl}\delta C_{mnj^\beta j}\rangle}{C^0_{j^\beta jj^\beta j}}P_{klmn}(k_\beta\hat{\boldsymbol{k}}),\quad P_{klmn}(k_\beta\hat{\boldsymbol{k}})=\int_{\mathbb{R}^{dim}}G_{km}(\boldsymbol{r})D_{ln}(\boldsymbol{r})\,d\boldsymbol{r}, \tag{4}$$

where G_{km} is the dyadic Green function in the 2D or 3D reference isotropic homogeneous medium, and its expression can be found in equations (16, 17) in [13] and $D_{ln}(\boldsymbol{r})=\frac{\partial^2}{\partial r_n\partial r_l}\left(W(\boldsymbol{r})e^{ik_\beta\hat{\boldsymbol{k}}\cdot\boldsymbol{r}}\right)$ is a second-order derivative tensor of the TPC spatial function. Using the Born approximation, with $k_\beta^2-k_{0\beta}^2\approx 2k_{0\beta}(k_\beta-k_{0\beta})$ and $k_\beta\approx k_{0\beta}$. The following expression is obtained for the wavenumber, valid in the 2D and 3D dimensions:

$$k_\beta=k_{0\beta}+\frac{k_{0\beta}}{2C_{j^\beta jj^\beta j}}\langle\delta C_{j^\beta jkl}\delta C_{mnj^\beta j}\rangle P_{klmn}(k_{0\beta}\hat{\boldsymbol{k}}). \tag{5}$$

The expression (5) is only valid in the Rayleigh and stochastic scattering regime due to the Born approximation. As can be seen, we consider the complex wavenumber in the heterogeneous medium as the sum of the wavenumber in the reference homogeneous medium plus a perturbation of that due to the grain's crystallographic and/or morphological heterogeneity. From this deviation, we can obtain the attenuation from the imaginary part $\alpha^\beta=\mathrm{Im}(k_\beta)$, and the phase velocity from the real part $V^\beta=\mathrm{Re}(k_\beta)$. In this work, we fix the wave propagation direction to be parallel to $\boldsymbol{e}_3$, therefore we have that $\hat{\boldsymbol{k}}=\boldsymbol{e}_3$. Also, we focus on the attenuation coefficient in 2D and 3D which can be both obtained from the following expressions:

$$\alpha^{\beta\gamma,2D}=\mathrm{Im}\left(\frac{k_{0\beta}\langle\delta C_{j^\beta jkl}\delta C_{mnj^\beta j}\rangle}{2C^0_{j^\beta jj^\beta j}}\int_{r=0}^{\infty}\int_{\theta=0}^{2\pi}G^\gamma_{km}(r,\theta)D^\beta_{ln}(r,\theta)r\,d\theta\,dr\right)\quad\beta,\gamma=L,T, \tag{6a}$$

$$\alpha^{\beta\gamma,3D}=\mathrm{Im}\left(\frac{k_{0\beta}\langle\delta C_{j^\beta jkl}\delta C_{mnj^\beta j}\rangle}{2C^0_{j^\beta jj^\beta j}}\int_{r=0}^{\infty}\int_{\theta=0}^{\pi}\int_{\varphi=0}^{2\pi}G^\gamma_{km}(r,\theta,\varphi)D^\beta_{ln}(r,\theta,\varphi)r^2\sin\theta\,d\varphi\,d\theta\,dr\right). \tag{6b}$$

The expressions (6a) and (6b) are valid for the general case of arbitrary crystal symmetry and grain shape. The integrals can be solved numerically using any available numerical integration library. The work of Bai *et al* [13] work already dealt with the case of microstructures with equiaxed grains and cubic crystal symmetry by considering an isotropic TPC spatial function of the form $W(r) = e^{-rd/2}$. In the present work, we still consider cubic crystal symmetry but we now deal with the case of microstructures with elongated grains.

In the 3D case, it can be assumed that the elongated grains have an ellipsoidal geometric shape. The assumed grain shape can be represented by the anisotropic TPC function (7), which is the extended form of the equiaxed TPC function. This function has already been used by [6], [7] and [8].

$$W(\boldsymbol{r}) = e^{-\sqrt{\boldsymbol{r}^T \boldsymbol{A} \boldsymbol{r}}}, \boldsymbol{A} = \sum_{i=1}^{3} \frac{1}{a_i^2} \boldsymbol{g}_i \otimes \boldsymbol{g}_i. \tag{7}$$

In equation (7), $\boldsymbol{A}$ is a second-order symmetric tensor composed by the inverse of a_1^2, a_2^2, a_3^2, which are the ellipsoidal radii in the local orthonormal coordinate system of the ellipsoid $(\boldsymbol{g}_1, \boldsymbol{g}_2, \boldsymbol{g}_3)$. In this particular work, we have that $a_1 \leq a_2 \leq a_3$. In the definition of $\boldsymbol{A}$, the rotation of the grain is implicit, with its basis depending on the angles τ and φ_τ. These angles define the orientation of the axis $\boldsymbol{g}_3$ as shown in Figure 1. In contrast with the development of Yang *et al* [7], here we fix the wave propagation direction, but we rotate the grain's principal axis $\boldsymbol{g}_3$. Both approaches are similar and interchangeable since the importance relies only on the angle between $\hat{\boldsymbol{k}}$ and $\boldsymbol{g}_3$.

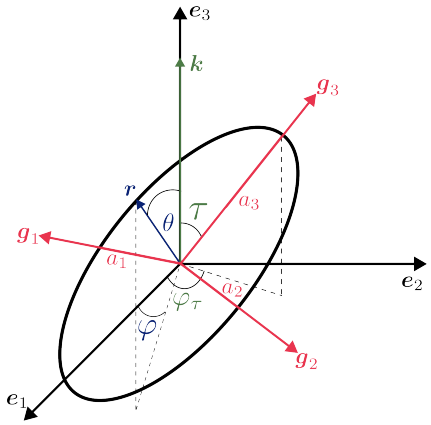

Figure 1. Illustration of an ellipsoidal grain, where a_1, a_2, a_3 are the ellipsoidal radii and τ, φ_τ are the orientation angles of the ellipsoid principal axis $\boldsymbol{g}_3$, and θ, φ are the angles of the vector $\boldsymbol{r}$.

The function (7) leads to:

$$\boldsymbol{D}^\beta(\boldsymbol{r}) = \left[-\frac{\boldsymbol{A}}{r} + \left(\frac{1}{r(\hat{\boldsymbol{r}}^T \boldsymbol{A} \hat{\boldsymbol{r}})} + \frac{1}{\sqrt{\hat{\boldsymbol{r}}^T \boldsymbol{A} \hat{\boldsymbol{r}}}} \right) (\boldsymbol{A}\hat{\boldsymbol{r}}) \otimes (\boldsymbol{A}\hat{\boldsymbol{r}}) - 2ik_{0\beta} \hat{\boldsymbol{k}} \otimes_s (\boldsymbol{A}\hat{\boldsymbol{r}}) - \sqrt{\hat{\boldsymbol{r}}^T \boldsymbol{A} \hat{\boldsymbol{r}}} k_{0\beta}^2 \hat{\boldsymbol{k}} \otimes \hat{\boldsymbol{k}} \right] \times \frac{e^{r\left(ik_{0\beta} \hat{\boldsymbol{k}} \cdot \hat{\boldsymbol{r}} - \sqrt{\hat{\boldsymbol{r}}^T \boldsymbol{A} \hat{\boldsymbol{r}}} \right)}}{\sqrt{\hat{\boldsymbol{r}}^T \boldsymbol{A} \hat{\boldsymbol{r}}}}, \tag{8}$$

where $r = \|\boldsymbol{r}\|$. We can define $R = a_3/a_1$ and $R_1 = a_2/a_1$ as the two aspect ratios of the ellipsoid. The grain can take any possible configuration in each axis of elongation $\boldsymbol{g}_3$ and $\boldsymbol{g}_2$ by tunning the ratios R and R_1 (cigar or pancake shape).

In the 2D case, one can start with an elongated 3D ellipsoidal grain and analyze a 2D cutting plane section defined by a unit vector $\hat{\boldsymbol{n}}$. A 2D plane with the same orientation vector $\hat{\boldsymbol{n}}$ in a 3D microstructure might cut the grains into multiple cross-sections. Here, we simplify by assuming that the 2D plane always cuts the grains at their center. The intersection of an ellipsoid and a cutting plane will always result in an ellipse or at least a sphere.

One can define a plane $\boldsymbol{t}_1, \boldsymbol{t}_2$ perpendicular to the defined normal unit vector $\hat{\boldsymbol{n}}$. As we decided to fix $\hat{\boldsymbol{k}} = \boldsymbol{e}_3$, we can set the axis $\boldsymbol{t}_2 = \hat{\boldsymbol{k}}$, and find $\boldsymbol{t}_1 = \hat{\boldsymbol{k}} \times \hat{\boldsymbol{n}}$. It can be found that $\boldsymbol{A}^{2D}$ can be written in terms of $\boldsymbol{A}^{3D}, \boldsymbol{t}_1, \boldsymbol{t}_2$ as:

$$\boldsymbol{A}^{2D} = \sum_{i,j=1}^{2} (\boldsymbol{t}_j \boldsymbol{A}^{3D} \boldsymbol{t}_i) \boldsymbol{t}_i \otimes \boldsymbol{t}_j. \tag{9}$$

Here, $\boldsymbol{A}^{2D}$ as in the 3D case, is a second-order symmetric tensor. It describes an ellipse in the orthonormal pair $\boldsymbol{t}_1, \boldsymbol{t}_2$. Since we decided to fix $\boldsymbol{t}_2 = \hat{\boldsymbol{k}} = \boldsymbol{e}_3$, the possible choices for $\hat{\boldsymbol{n}}$ are reduced to the options lying in the global coordinate system plane $\boldsymbol{e}_1, \boldsymbol{e}_2$. By rotating $\hat{\boldsymbol{n}}$ several ellipsoidal cross-sections are possible to obtain, allowing a direct 2D and 3D comparison and analysis of the ultrasonic attenuation dimensionality.

3. Results and discussion on the relationship attenuation-grain shape in 2D and 3D

3.1. Comparison between 3D and 2D theoretical attenuation similarities and differences

We start by comparing the 3D and 2D theoretically estimated ultrasonic attenuation in Titanium (Beta phase) for which the material constants are presented in Table 1. The main idea is to analyze the influence of the grain's orientation and the dimensionality in the attenuation. For this purpose, we consider a grain with average radii $a_1 = 0.1\ mm, a_2 = 2a_1, a_3 = 5a_1$. Additionally, we consider three different grain rotations (a), (b) and (c) as presented in Table 2. Moreover, we consider three choices (I, II, III as shown in Table 2) of the unit normal vector $\hat{\boldsymbol{n}}$, representing three different 2D slices for each 3D case.

Table 1. Elastic constants (GPa) and material properties of the Titanium (Beta phase) and the reference medium.

	C_{1111}	C_{1122}	C_{1212}	ϵ_L	ϵ_T	$\rho\ (kg/m^3)$
Titanium (Beta phase)	134.0	110.0	36.0	2.74×10^{-2}	1.19×10^{-1}	4428
Reference medium (Voigt average)	153.0	100.0	26.5	0	0	4428

Table 2. Ellipse cross-section area (mm^2) and grain radius $a_{||}$ (mm) resulting from each selected normal plane for the three considered grain orientations.

	(I) $\hat{\boldsymbol{n}} = \boldsymbol{e}_1$	(II) $\hat{\boldsymbol{n}} = \boldsymbol{e}_2$	(III) $\hat{\boldsymbol{n}} = \frac{1}{\sqrt{2}}(\boldsymbol{e}_1 + \boldsymbol{e}_2)$	$a_{\|\|}$
(a) $\boldsymbol{g}_1 = \boldsymbol{e}_1, \boldsymbol{g}_2 = \boldsymbol{e}_2, \boldsymbol{g}_3 = \boldsymbol{e}_3$	$\pi/10$	$\pi/20$	$\pi/15.81$	0.5
(b) $\boldsymbol{g}_1 = \boldsymbol{e}_3, \boldsymbol{g}_2 = \boldsymbol{e}_1, \boldsymbol{g}_3 = \boldsymbol{e}_2$	$\pi/20$	$\pi/50$	$\pi/38.08$	0.1
(c) $\boldsymbol{g}_1 = \boldsymbol{e}_1, (\boldsymbol{g}_2, \boldsymbol{e}_2) = 1/\sqrt{2}, (\boldsymbol{g}_3, \boldsymbol{e}_3) = 1/\sqrt{2}$	$\pi/10$	$\pi/38.08$	$\pi/27.84$	0.35

Figure 2 presents the 3D and 2D comparison of the obtained theoretical results. The obtained master curve of the attenuation coefficient α_L in 3D is comparable to that of previous works [6], [7] and [8]. In the Rayleigh scattering regime, the 3D longitudinal normalized attenuation depends on the grain average volume and has a power behavior of $\alpha_L^{3D} d \propto (fd)^4$, where d is the grain diameter in any axis of elongation. In contrast, the 2D normalized attenuation shows a clear cross-section dependency $\alpha_L^{2D} d \propto (fd)^3$ which can be seen explicitly. Looking at each 2D normalized curve one can see that the curve with higher values of attenuation belongs to the planes with a higher cross-section area (I)>(III)>(II) for all three rotations (a), (b) and (c).

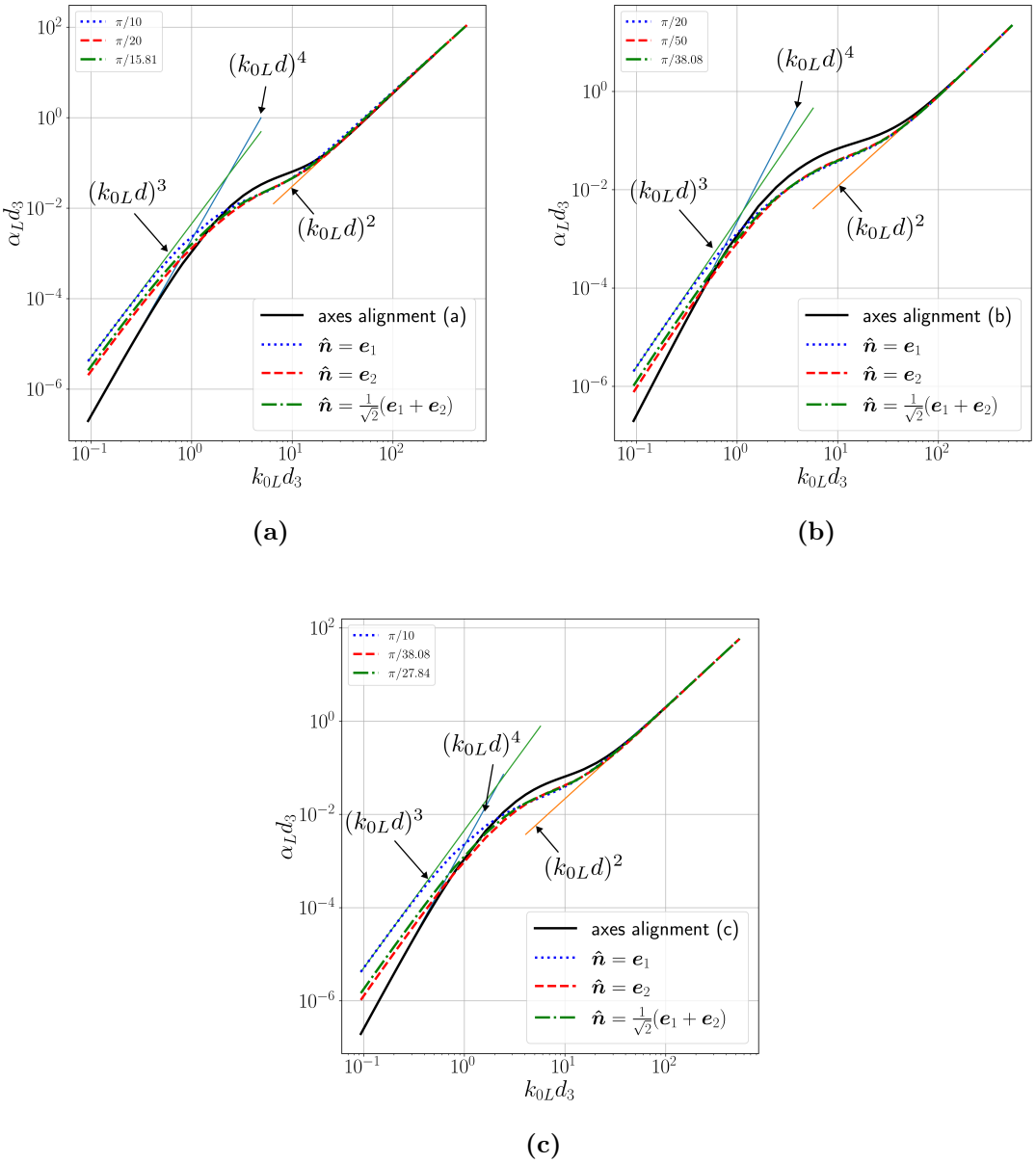

Figure 2. Normalized 3D and 2D attenuation curves with $d_3 = 2a_3$ for a grain with three rotations corresponding to those presented in Table 2 (a), (b) and (c) respectively.

At the stochastic scattering regime, the longitudinal normalized attenuation in 3D and 2D

are dependent on $d_{||} = 2a_{||}$ the grain size parallel to the wave propagation direction $\hat{\boldsymbol{k}}$. For each case (a), (b) and (c), for each 2D normalized curve, despite the chosen plane (I), (II) or (III), the grain size parallel to $\hat{\boldsymbol{k}}$ remains equal (see Table 2); therefore convergence to the same attenuation values from the Rayleigh to the stochastic regime in the 3D and 2D dimensions is obtained. This last behavior shows that the attenuation in the stochastic frequency regime is mostly a 1D phenomenon of longitudinal to longitudinal wave scattering and therefore easily predicted by the 2D and 3D theoretical models. Figure 3a shows the comparison of the longitudinal normalized attenuation for the 3D case. It helps to visualize, that for a larger value of $a_{||}$ ((a)>(b)>(c) see Table 2 and Figure 3a), higher values of attenuation are reached.

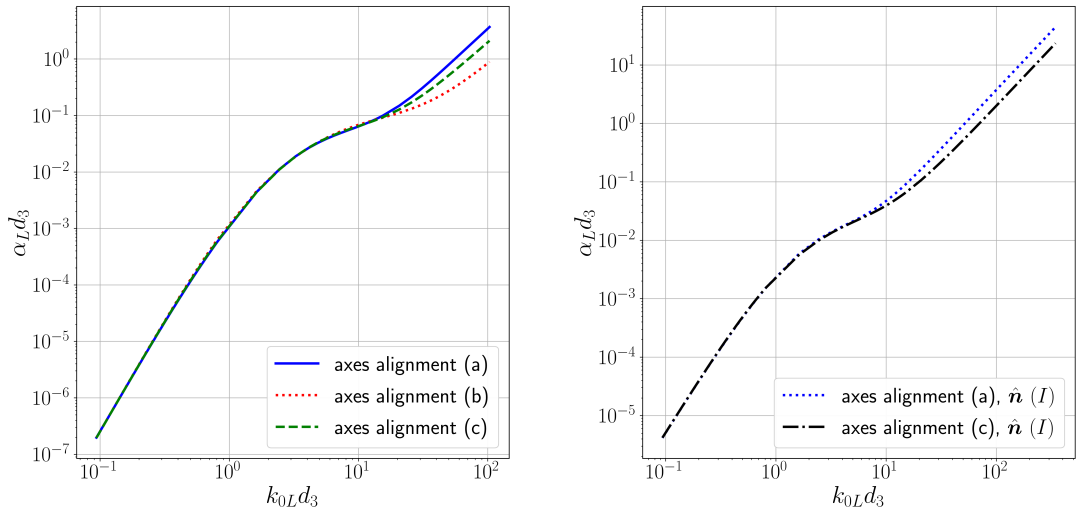

(a) **(b)**

Figure 3. Comparison of the longitudinal normalized attenuation for (a) the 3D grain with the three different chosen rotations and (b) the 2D grain resulting from the normal plane (I) for the grain rotations (a) and (b) (see Table 2).

In the Rayleigh-to-stochastic transition regime, the 3D attenuation takes higher values than the 2D attenuation in each case (Figure 2), the same behavior as in the case of the equiaxed grains described by Bai *et al* [13]. Figure 3b compares the longitudinal normalized attenuation for the normal plane (I) for the rotations (a) and (c). It is interesting to notice that the cases (a.I) and (c.I) (see Table 2) have the same cross-section area due to the axes alignment chosen and therefore both curves (a.I) and (c.I) take the same attenuation values in the lower frequency domain. Nevertheless, it can be appreciated that at the stochastic scattering regime, curve (a.I) takes considerably higher attenuation values than curve (c.I). This demonstrates the dependency on the grain's rotation in the higher frequency domain.

3.2. 3D grain shape from 2D ultrasonic attenuation

Figure 4 presents the polar plot of the longitudinal normalized attenuation in the 2D dimension versus the angle of rotation of the normal unit vector $\hat{\boldsymbol{n}}$ measured from the axis $\boldsymbol{e}_1$ as it rotates in the anti-clockwise direction for the 3D grain considered previously with axes orientation (a) as in Table 2. It presents three different normalized frequencies corresponding to the Rayleigh scattering regime 4a, the transition regime 4b and the stochastic regime 4c. In the Rayleigh scattering regime we can see more clearly the cross-section dependency as $\hat{\boldsymbol{n}}$ moves from 0° the

maximum cross-section for the ellipse with axes $(\boldsymbol{g}_2, \boldsymbol{g}_3)$ to 90° the minimum cross-section for the ellipse with axes $(\boldsymbol{g}_1, \boldsymbol{g}_3)$. As the frequency increases it is clear this dependency vanishes as the normalized frequency approaches the limit of the stochastic scattering regime.

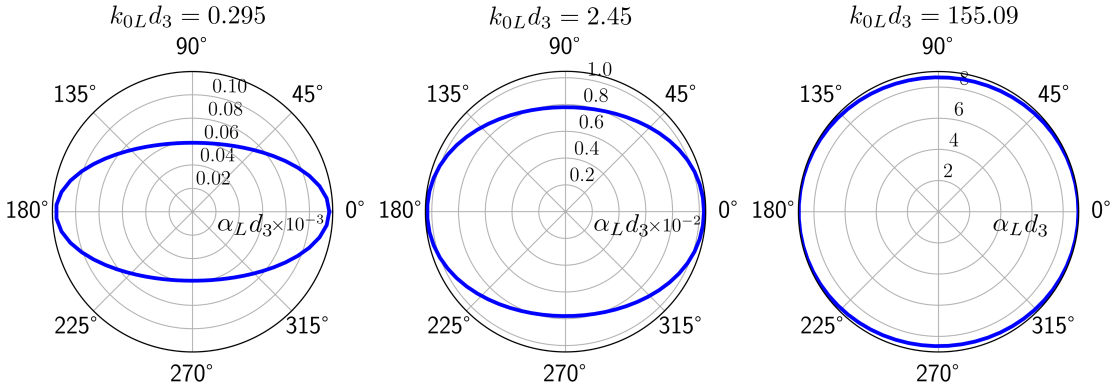

(a) **(b)** **(c)**

Figure 4. Polar plot of the normalized longitudinal attenuation in the 2D dimension versus the angle of the normal unit vector $\hat{\boldsymbol{n}}$ measured from the axis $\boldsymbol{e}_1$ for a 3D grain with $a_3 = 5a_1, a_2 = 2a_1$, for the normalized frequencies k_{0Ld_3} of (a) 0.295, (b) 2.45 and (c) 155.09.

We want to point out that it is interesting that in the Rayleigh scattering regime (Figure 4a), the attenuation gives an implicit idea of the grain cross-section shape. For instance, knowing that in the lower frequency domain, the minimum values of attenuation correspond to the maximum cross-section area, it can be interpreted from the polar plot, the elongated axis in the plane parallel to $\hat{\boldsymbol{n}}$. In the case of Figure 4a (plane $\boldsymbol{e}_1 - \boldsymbol{e}_2$), the elongated axis $\boldsymbol{g}_2$ is parallel to $\boldsymbol{e}_2$ (90° in the polar plot).

To better illustrate this, Figure 5a plots the inverse of the 2D attenuation normalized by d_3 for three different planes of rotation for $\hat{\boldsymbol{n}}$, case (i) $\hat{\boldsymbol{n}}$ belongs to the plane P_{12} formed by $\boldsymbol{e}_1, \boldsymbol{e}_2$, case (ii) plane P_{23} formed by $\boldsymbol{e}_2, \boldsymbol{e}_3$ and case (iii) plane P_{13} formed by $\boldsymbol{e}_1, \boldsymbol{e}_3$. Last, case (iv) for a 3D grain with the same radii as considered before but with $\boldsymbol{g}_2$ rotated by 45° with respect to the axis e_1. The abovementioned planes of rotation are chosen with the intention of "scanning" a 3D grain from its three planes. First, we can see in case (iv) (plot 5a) that by looking at the inverse of the attenuation, we can indicate the grain's elongated axis 135° and the short axis 45° in the plane of $\hat{\boldsymbol{n}}$. Then, it follows that by "scanning" one single 3D grain from its three different planes, one can have an idea of the full 3D grain shape by the 2D attenuation in the Rayleigh scattering regime. Now we can come back to the 3D grain aligned with the global axes. We can start by studying the case (i), at 0° $\hat{\boldsymbol{n}} = \boldsymbol{e}_1$ the cross-section is composed by the two remaining axes $\boldsymbol{e}_2, \boldsymbol{e}_3$, then at 90° $\hat{\boldsymbol{n}} = \boldsymbol{e}_2$, the cross-section is composed by $\boldsymbol{e}_1, \boldsymbol{e}_3$. Since the wave propagation direction $\hat{\boldsymbol{k}} = \boldsymbol{e}_3$, then the only difference between the maximum and minimum attenuation relies on the gain's radius in the perpendicular axis $\boldsymbol{e}_1$ or $\boldsymbol{e}_2$. Therefore, from the polar plot (case (i) Figure 5a) we can infer that the grain's radii $a_{90} > a_0$ in the plane of $\hat{\boldsymbol{n}}$. We can continue with the same analysis for the other two planes of inspection. In case (ii) we choose $\hat{\boldsymbol{n}} \in P_{23}$ and rotate it in the anti-clockwise sense from the axis $\boldsymbol{e}_2$. We again can see the same behavior, at 0° the resulting ellipse is composed by the axes $\boldsymbol{e}_1, \boldsymbol{e}_3$ and at 90° by the axes $\boldsymbol{e}_1, \boldsymbol{e}_2$, therefore $a_{90} > a_0$ (see Figure 5a). The same analysis applies to case (iii) from which we can deduce $a_{90} > a_0$. In the latter, we also see the coincidence at 0° with case (i) and at 90° with case (ii). Finally, considering all three cases (i-iii) together one can arrive to the conclusion that $a_{0_{\text{ii}}} > a_{0_{\text{iii}}} > a_{0_{\text{i}}}$ and that $a_{90_{\text{iii}}} = a_{90_{\text{ii}}} > a_{90_{\text{i}}}$. Then by correlation of the angles of rotation and the planes of $\hat{\boldsymbol{n}}$, one can see that $a_{90_{\text{iii}}} = a_{90_{\text{ii}}} = a_3$, $a_{0_{\text{ii}}} = a_{90_{\text{i}}} = a_2$ and $a_{0_{\text{ii}}} = a_{0_{\text{i}}} = a_1$, thus

$a_3 > a_2 > a_1$.

In addition to the obvious influence of the elongated and short radii in the normalized polar plot of attenuation, we can also see a proportionality of the ratio of attenuation in the shortest/elongated axes and the aspect ratio of the grain R, for a value of a_1 and fixing $R_1 = 1$. This is an expected relation due to the already determined cross-section dependency. To show this proportionality we decided to compute the ratio of the attenuation at 90° in the cases $\hat{\boldsymbol{n}} \in P_{12}$ and $\hat{\boldsymbol{n}} \in P_{23}$ for grain with increasing R and constant $R_1 = 1$ for three different values of a_1 ($0.1\ mm, k_{0L}d_1 = 0.0590$, $0.05\ mm, k_{0L}d_1 = 0.0295$ and $0.01\ mm, k_{0L}d_1 = 0.0059$ in Figure 5b). This setting finally results in a comparison of the attenuation when the wave propagates in the elongated axis a_3 and short axis $a_1 = a_2$. Figure 5b presents a plot of the ratio of the attenuation in the shortest and elongated direction versus the ratio R/R_1 for a constant value of $R_1 = 1$. This plot shows, first of all, an explicit proportional relationship with slop equal to 1 between the ratio of attenuation and the ratio of elongated/short radii as the average equivalent grain size approaches the limit of the Rayleigh scattering regime. But also, in the plot we decided to show the normalized frequency with d_1 to have an idea of the order of the grain equivalent size and show that as the normalized frequency approaches the limit of the Rayleigh scattering regime (a_1 decreases), this proportionality tends to a $1:1$ behavior. As for the three curves presented, we have that for the attenuation in the elongated radii $\hat{\boldsymbol{k}} = \boldsymbol{e}_3$, we should be looking at the normalized frequency $k_{0L}d_3$ but as we have that d_3 varies, we skip it for clarity. Nevertheless, we can see clearly in the case of $k_{0L}d_1 = 0.0590$ (higher equivalent grain size) that as R increases, and therefore d_3 increases the grain size/wavelength ratio increases and moves upwards in the normalized frequency regime, and therefore the proportionality $1:1$ seen at lower equivalent grain size (lower R) starts to decrease.

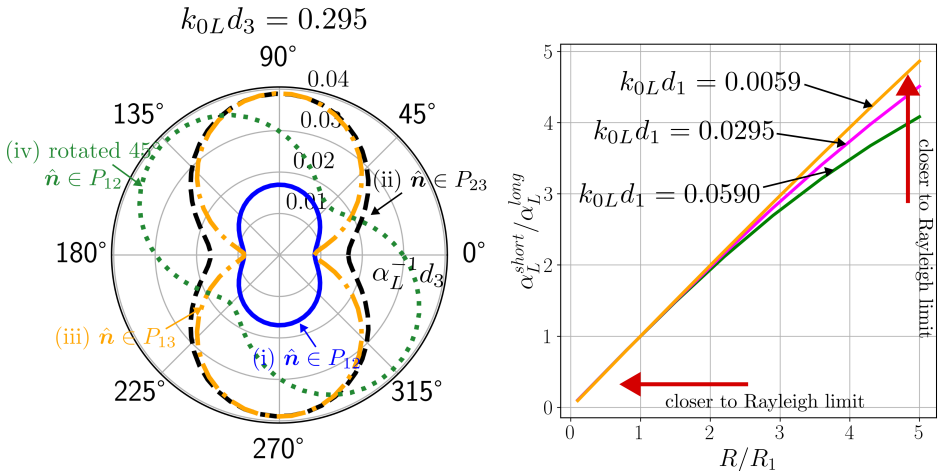

(a) **(b)**

Figure 5. (a) Polar plot of the longitudinal normalized attenuation for (i) $\hat{\boldsymbol{n}} \in P_{12}$, (ii) $\hat{\boldsymbol{n}} \in P_{23}$, (iii) $\hat{\boldsymbol{n}} \in P_{13}$ and (iv) $\hat{\boldsymbol{n}} \in P_{12}$ for a grain rotated 45°. (b) Ratio of the longitudinal attenuation when $\hat{\boldsymbol{k}}$ propagates along the shortest and elongated axis versus the ratio R/R_1 for $R_1 = 1$ and three different values of a_1 $[0.1, 0.05, 0.01]$ mm resulting in three different values of normalized $k_{0L}d_1$ $[0.0590, 0.0295, 0.0059]$.

4. Conclusions and perspectives

A theoretical model for the ultrasonic attenuation in 3D and 2D untextured single-phase microstructures with elongated grains and cubic crystal symmetry has been developed in the

Born approximation. The 2D model was developed with the idea of capturing different and selected specific cross-sections of a single 3D grain. The attenuations of the longitudinal wave predicted by the 2D and 3D models are compared for an anisotropic grain. A deeper analysis in the 2D case was made to exhibit a relation between the 3D grain shape and the attenuation of the longitudinal wave in the Rayleigh scattering regime. The longitudinal attenuation in the 2D case was found to be proportional to the cross-section (power law of f^3), in contrast to the 3D case which shows a volume dependency and a frequency dependency of f^4 in the Rayleigh scattering regime. In the stochastic scattering regime, both in 3D and 2D cases, the attenuation was found to be dependent on the grain size parallel to the wave propagation direction $\hat{\boldsymbol{k}}$ (power law of f^2). It was shown that in the Rayleigh scattering regime, the attenuation calculated from 2D cross-sections can be useful to locate the elongated and shortest axes of the 3D grain. It is an interesting result since the 3D attenuation in the Rayleigh scattering regime is only volume dependent which makes it difficult in the lower frequency domain to have an idea of the grain shape. Moreover, it was also found that the ratio $\alpha_L^{short}/\alpha_L^{elongated} \propto R/R_1$ and it follows a linear relationship when the relation grain size/wavelength approaches the limit of the Rayleigh scattering regime. These two results together can give an idea of the axes of elongation of the grain of ellipsoidal shape and also the grain's aspect ratio using low-frequency signals, when it is intended to be used in inverse methods for microstructure characterization.

Acknowledgments
This work was part of Juan Camilo Victoria Giraldo's doctoral study. The authors are also grateful for funding provided by the Agence Nationale de la Recherche (No. ANR-21-CE08-0026, Research Project COLUMBO). Computations were performed using HPC resources from the "Mésocentre Paris-Saclay", a computing center of Paris-Saclay University.
[14]

References

[1] Arguelles A P, Kube C M, Hu P and Turner J A 2016 *J. Acoust. Soc. Am.* **140** 1570–1580 ISSN 0001-4966 URL http://asa.scitation.org/doi/10.1121/1.4962161

[2] Arguelles A P and Turner J A 2017 *J. Acoust. Soc. Am.* **141** 4347–4353 ISSN 0001-4966, 1520-8524 URL https://pubs.aip.org/jasa/article/141/6/4347/915703/Ultrasonic-attenuation-of-polycrystalline

[3] Stanke F E and Kino G S 1984 *J. Acoust. Soc. Am.* **75** 665–681 ISSN 0001-4966 URL http://asa.scitation.org/doi/10.1121/1.390577

[4] Karal Jr F C and Keller J B 1964 *J. Math. Phys.* **5** 537–547 ISSN 0022-2488, 1089-7658 URL http://aip.scitation.org/doi/10.1063/1.1704145

[5] Weaver R L 1990 *J. Mech. Phys. Solids* **38** 55–86 ISSN 00225096 URL https://linkinghub.elsevier.com/retrieve/pii/002250969090021U

[6] Ahmed S 2003 *AIP Conference Proceedings* vol 657 (Bellingham, Washington (USA): AIP) pp 109–116 iSSN: 0094243X URL http://aip.scitation.org/doi/abs/10.1063/1.1570126

[7] Yang L, Lobkis O and Rokhlin S 2011 *Ultrasonics* **51** 697–708 ISSN 0041624X URL https://linkinghub.elsevier.com/retrieve/pii/S0041624X11000266

[8] Calvet M and Margerin L 2016 *Wave Motion* **65** 29–43 ISSN 01652125 URL https://linkinghub.elsevier.com/retrieve/pii/S0165212516300063

[9] Huang M, Sha G, Huthwaite P, Rokhlin S I and Lowe M J S 2020 *J. Acoust. Soc. Am.* **148** 1890–1910 ISSN 0001-4966 URL http://asa.scitation.org/doi/10.1121/10.0002102

[10] Huang M, Sha G, Huthwaite P, Rokhlin S I and Lowe M J S 2021 *J. Acoust. Soc. Am.* **149** 2377–2394 ISSN 0001-4966 URL https://asa.scitation.org/doi/10.1121/10.0003955

[11] Van Pamel A, Brett C R, Huthwaite P and Lowe M J S 2015 *J. Acoust. Soc. Am.* **138** 2326–2336 ISSN 0001-4966 URL http://asa.scitation.org/doi/10.1121/1.4931445

[12] Bai X 2017 *Modélisation par éléments finis de la propagation des ondes ultrasonores dans des matériaux polycristallins* Ph.D. thesis Université Paris-Saclay (ComUE) URL https://theses.hal.science/tel-01483701

[13] Bai X, Tie B, Schmitt J H and Aubry D 2020 *Ultrasonics* **100** 105980 ISSN 0041624X URL https://linkinghub.elsevier.com/retrieve/pii/S0041624X18308096

[14] Wilcox L C, Stadler G, Burstedde C and Ghattas O 2010 *Journal of Computational Physics* **229** 9373–9396 ISSN 00219991 URL https://linkinghub.elsevier.com/retrieve/pii/S0021999110005024